Letter   **Editors' Suggestion**

Identifying a critical micelle temperature in simulations of disordered asymmetric diblock copolymer melts

Anshul Chawla ⓘ, Frank S. Bates ⓘ, Kevin D. Dorfman ⓘ,[*] and David C. Morse ⓘ[†]

Department of Chemical Engineering and Materials Science, University of Minnesota, 421 Washington Avenue SE,
Minneapolis, Minnesota 55455, USA

Experiments on asymmetric diblock copolymers at temperatures slightly above the order-disorder transition (ODT) temperature indicate the existence of a dense fluid of micelles. Molecular dynamics simulations are used here to identify a higher critical micelle temperature below which micelles appear. The onset of micellization occurs very near where self-consistent field theory predicts an ODT.

In melts of highly asymmetric diblock copolymers at temperatures slightly above the order-disorder transition (ODT) temperature, the disordered phase contains a dense liquid of spherical micelles [1–7]. At the ODT, these micelles crystallize. Simple analogies to the theory of binary surfactant-solvent mixtures, which exhibit a critical micelle concentration [8], suggest that a micelle-forming one-component system should exhibit a critical micelle temperature (CMT) at which micelles appear with decreasing temperature over a rather narrow range of temperatures [9,10]. The ODT is clearly identifiable in scattering experiments by the appearance of Bragg peaks. Clear experimental identification of a CMT has, however, remained elusive.

In this Letter, we study the appearance of micelles in large-scale simulations of a coarse-grained simulation model of *AB* diblock copolymers with well-characterized thermodynamic properties and an experimentally relevant chain length. Simulations allow access to information about molecular clusters that is not easily accessible in experiments. We confirm that spherical micelles do indeed appear and proliferate over a narrow range of temperatures, and show that this occurs very near where self-consistent field theory (SCFT) predicts the simultaneous emergence and crystallization of micelles.

Micelle formation in compositionally asymmetric block copolymers bears similarities to the formation of a disordered bicontinuous morphology above the ODT in symmetric block copolymers. Both are manifestations of strong correlations in the disordered phase, which critically influence order-disorder transitions in finite molecular weight systems [11–15], although many aspects of both structure and dynamics are qualitatively different. Whereas the bicontinuous state has recently been described theoretically [16–18] and imaged using electron microscopy [19–22], micelle formation, and the existence of a CMT, remains largely unexplored notwithstanding the publication of several provocative transmission electron

microscopy (TEM) images two decades ago [5,6]. The importance of this ubiquitous state of condensed matter has become increasingly evident with the discovery of dodecagonal quasicrystals and numerous Frank-Kasper phases in a host of soft materials [13,23–30]. Recent reports of metastable particle-based phases that evolve from the quenched disordered liquid [31–33] underscore the significance of this unique, and poorly understood state, motivating the work described here.

Experimental evidence for the existence of micelles in the disordered phase comes primarily from microscopy and scattering experiments. The most direct evidence is from transmission electron micrographs showing disordered arrangements of spherical micelles [5,6]. Results of small-angle x-ray (SAXS) and neutron (SANS) scattering from the disordered phase near the ODT exhibit a secondary shoulder in plots of scattered intensity $I(q)$ versus wave number q, at a wave number well above the primary peak wave number q^*. This secondary feature is believed to be a consequence of liquidlike correlations in micelle positions, and has been successfully modeled using liquid-state theories for hard spheres [1–4,7].

The quantitative understanding of self-assembly in sphere-forming systems relies heavily on predictions of self-consistent field theory (SCFT) [13,31,34–38]. Consider a melt of *AB* diblock copolymers with a volume fraction $f < 0.2$ for the minority *B* block, an overall degree of polymerization N, Flory-Huggins parameter χ, monomer concentration c, and statistical segment length b for both *A* and *B* monomers. SCFT predicts that micelles should both appear and crystallize at a transition value of χN, denoted here by $(\chi N)_{\text{odt}}^{\text{scf}}$. SCFT is believed to be exact in the limit of infinite invariant degree of polymerization $\overline{N} = N(cb^3)^2$ [11,16,17,39], but ignores the existence of strong correlations in the disordered phase in systems with experimentally relevant molecular weights.

Wang *et al.* [10] have used SCFT to compute the free energy of formation for an isolated spherical micelle within a disordered phase, denoted by W_m. SCFT yields a prediction of the form $W_m = k_B T \overline{N}^{1/2} \tilde{W}_m(\chi N, f)$, where $\tilde{W}_m$ is a dimensionless function of χN and f. The value of χN above which $W_m < 0$ at a given f, denoted here by $(\chi N)_{\text{m}}^{\text{scf}}$, is found to be

very near to but slightly greater than $(\chi N)_{\mathrm{odt}}^{\mathrm{scf}}$. For example, for $f = 0.1$, $(\chi N)_{\mathrm{odt}}^{\mathrm{scf}} = 47.95$ and $(\chi N)_{\mathrm{m}}^{\mathrm{scf}} = 48.14$ [10]. This small difference is a result of a weak attraction between micelles in a crystal, but is negligible for purposes of the analysis given here. SCFT predicts the existence of strongly segregated micelle cores even at $(\chi N)_{\mathrm{odt}}^{\mathrm{scf}}$, with a minority volume fraction near 90% at the center of the micelle for $f \simeq 0.1$. Upon allowing for micelle translational entropy, Wang *et al.* predict a micelle volume fraction proportional to $e^{-W_m/k_B T}$ and a rapid increase in micelle concentration over a narrow range of values of χN of width $\overline{N}^{-1/2}$ near $(\chi N)_{\mathrm{m}}^{\mathrm{scf}}$. These conclusions are consistent with those of an earlier analysis by Dormidontova and Lodge [9] that relied on a less accurate strong segregation model for W_m, but that allowed for effects of micelle interactions that Wang *et al.* neglected. While these theoretical predictions are enticing, neither experiments nor simulations have thus far allowed a definitive identification of a CMT in compositionally asymmetric diblock copolymers.

Recent progress in the interpretation of coarse-grained molecular simulations has enabled increasingly precise comparisons of simulations to SCFT, and thereby sharpened our understanding of the strengths and weaknesses of SCFT. The comparison to SCFT predictions given here was enabled by this prior work. Glaser, Medapuram, Morse, and co-workers introduced a method of calibrating the dependence of the effective χ parameter on simulation input parameters that has allowed consistent results to be obtained from a variety of different coarse-grained models [16,17,40–43]. Their analysis showed that strong correlations appear within the disordered phase when χN exceeds $(\chi N)_{\mathrm{odt}}^{\mathrm{scf}}$, while the actual ODT occurs at an elevated value $(\chi N)_{\mathrm{odt}}$ that exhibits a universal dependence on $\overline{N}$. Notably, SCFT was found to yield rather accurate predictions for properties of ordered lamellar and hexagonal phases [16,17,43]. These results thus provided evidence for the accuracy of SCFT predictions for self-assembled structures such as lamellae or micelles, while also emphasizing the failure of a random-mixing description of the disordered phase near the ODT. The assumption that SCFT accurately predicts the free energy required to form an isolated micelle also suggests a hypothesis that micelles should first appear at a value of χN very near $(\chi N)_{\mathrm{odt}}^{\mathrm{scf}}$.

In this Letter, we study the appearance of micelles in molecular dynamics (MD) simulations of an AB diblock copolymer melt. Simulations are performed in a constant pressure, constant temperature ensemble. A quantitative comparison to theoretical predictions is enabled by using a simulation model for which the relationship between χ and simulation parameters has been established previously [16,17]. The model used here is referred to as model S2 in Refs. [16,17] or model D3 in Ref. [42], for which $\overline{N}/N = (cb^3)^2 = 59.7$. In all work reported here, each chain has $N = 64$ beads, with eight B beads and 56 A beads, giving $f = 1/8$ and $\overline{N} = 3820$. SCFT predicts $(\chi N)_{\mathrm{odt}}^{\mathrm{scf}} = 36.6$ for $f = 1/8$. A harmonic bond potential acts between adjacent beads within each chain. A nonbonded pair potential of the form $V(r) = \frac{1}{2}\epsilon_{ij}(1 - r/\sigma)^2$ acts between beads of types i and j that are separated by a distance r less than a cutoff σ, with $V(r) = 0$ for $r > \sigma$. The parameter $\alpha = (\epsilon_{AB} - \epsilon_{AA})/k_B T$ is varied to modify the effective χ parameter, while the pressure, temperature, bond spring constant, and $\epsilon_{AA} = \epsilon_{BB}$ are held at constant
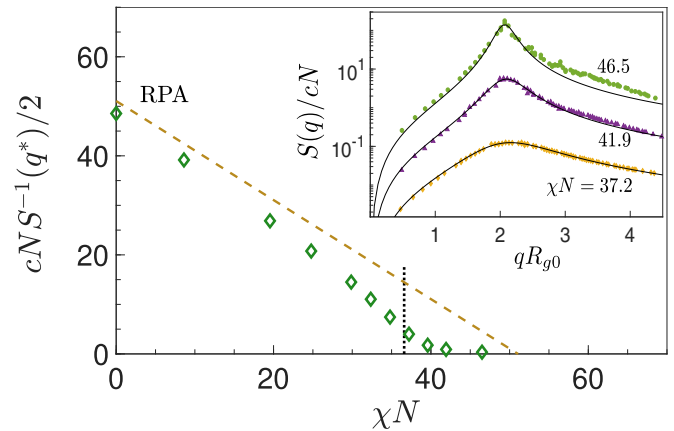

FIG. 1. Main plot: Nondimensional inverse peak intensity $cNS^{-1}(q^*)/2$ vs χN. The dashed line shows the RPA prediction. The dotted vertical line indicates $(\chi N)_{\mathrm{odt}}^{\mathrm{scf}} = 36.6$. Inset: Structure factor $S(q)$ vs qR_{g0} at three nearby values of χN, where $R_{g0} = b\sqrt{N/6}$. Solid lines show a fit to the RPA functional form.

values chosen in previous work. Simulations were performed on systems of approximately 5×10^5 beads. Further simulation details are given in the Supplemental Material [44].

Figure 1 shows the behavior of the structure factor $S(q)$, akin to the scattering intensity measured in SAXS and SANS experiments. We define $S(q) = V^{-1}\langle|\psi(\mathbf{q})|^2\rangle$, where $\psi(\mathbf{q}) = \int d\mathbf{r}\,\psi(\mathbf{r})e^{i\mathbf{q}\cdot\mathbf{r}}$, $\psi(\mathbf{r}) = [c_A(\mathbf{r}) - c_B(\mathbf{r})]/2$, $c_i(\mathbf{r})$ is the concentration of i monomers, V is system volume, and $q = |\mathbf{q}|$. All values of χN reported in this Letter were calculated using a calibration of χ obtained in previous work [16,17] (see Table S1).

The inset of Fig. 1 shows $S(q)$ vs q at three values of χN near $(\chi N)_{\mathrm{odt}}^{\mathrm{scf}} = 36.6$. Solid lines show fits of $S(q)$ to a functional form $S(q) = KS_{\mathrm{RPA}}(q)$, in which $S_{\mathrm{RPA}}(q)$ is the random-phase approximation (RPA) prediction, and in which R_g, χ, and the prefactor K have all been treated as adjustable parameters. A comparison to this fit helps emphasize the existence at $\chi N = 46.5$ and 41.9 of a weak shoulder in $S(q)$ at $qR_{g0} \simeq 3.4$, which we identify here by the failure of an attempted fit to the RPA. This feature is absent for all $\chi N < (\chi N)_{\mathrm{odt}}^{\mathrm{scf}}$, for which $S(q)$ is fit well by the RPA functional form. An analogous feature has been observed in scattering scattering experiments performed at temperatures slightly above the ODT [1–3,6,7], which appears at wave numbers with approximately the same relationship to the peak wave number as that found here, though the magnitude of this secondary feature varies in experiments depending on proximity to the ODT and $\overline{N}$.

The main plot in Fig. 1 shows the behavior of the normalized inverse of the peak intensity $cNS^{-1}(q^*)/2$ vs χN. The dashed line shows the RPA prediction for this quantity, computed without adjustable parameters. The actual dependence of $S^{-1}(q^*)$ on χN shows a falling point of inflection near $(\chi N)_{\mathrm{odt}}^{\mathrm{scf}}$ that separates a region of slight negative curvature at lower χN from a region of positive curvature at higher χN. Notably, this behavior is different from that found in symmetric and modestly asymmetric copolymers, for which this plot instead exhibits a uniformly positive curvature,
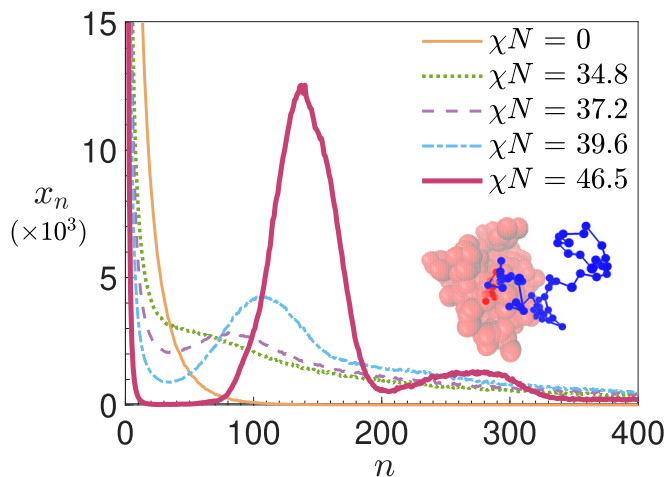
FIG. 2. Average mole fraction x_n of chains within clusters of aggregation number n, vs n. The inset shows a cluster snapshot, with B (core) beads in translucent red, with one chain highlighted with blue A beads and red B beads.

reflecting the tendency of $S(q^*)$ to increase more slowly with increasing χN than predicted by the RPA. The behavior seen here instead indicates a tendency for $S(q^*)$ to increase more rapidly than predicted by the RPA for χN near $(\chi N)_{\mathrm{odt}}^{\mathrm{scf}}$. An alternative view of these data is shown in Fig. S1 by plotting $S(q^*)/S_{\mathrm{RPA}}(q^*)$ vs χN, which shows a rapid increase near $(\chi N)_{\mathrm{odt}}^{\mathrm{scf}}$. We show below that this increased scattering coincides with the appearance of micelles.

In an MD simulation, potential micelles may be identified by finding clusters of molecules with minority B block beads in close contact. We identify such clusters using a criterion in which two molecules are taken to belong to the same cluster if the distance between any two B beads on these different molecules is less than 0.8σ. Let n denote the number of molecules in such a cluster.

Figure 2 shows the fraction x_n of chains within clusters of aggregation number n plotted versus n at several values of χN. At $\chi N = 0$, geometrical clusters exist only as a result of random intermolecular minority block contacts. In this limit, x_n decreases monotonically with increasing n but still includes a non-negligible value for clusters with tens of molecules. The distribution evolves slowly with increasing χN up to the next displayed value of $\chi N = 34.8$, which is slightly less than $(\chi N)_{\mathrm{odt}}^{\mathrm{scf}} = 36.6$. At this value, x_n remains monotonically decreasing but shows an enhanced frequency for larger n as a result of increasingly strong composition fluctuations. For $\chi N \geqslant 37.2$, however, the distribution develops a local maximum at a most probable aggregation number $n^* \simeq 80$–140 that grows larger and more distinct with increasing χN, signaling the appearance of proper micelles. We will show in a future publication that the secondary maximum at $n \simeq 2n^* \simeq 280$ at $\chi N = 46.5$ is due to clusters containing two micelles with cores joined by a narrow throat.

Figure 3 describes the spatial structure of clusters with aggregation numbers within a range chosen to correspond to potential micelles. At values of χN for which the plot of x_n vs n from Fig. 2 shows a local maximum, properties in Fig. 3 are computed by considering clusters with n ranging from the least probable value (the minimum in Fig. 2) to 1.6 times the most probable value. A range of $n = 30$–160 is instead used at lower values of χN for which no local maximum exists.

Figure 3(a) shows the average $\overline{\phi}_B(r)$ of the effective volume fraction $\phi_B(r)$ of B (minority) beads that belong to a cluster as a function of distance r from the center of mass (COM) of all B beads in the cluster. We define the value of ϕ_B within a small region of volume ΔV to be equal to a ratio $\phi_B = m_B/c\Delta V$, where m_B is the number of B beads in that region that belong to molecules in a cluster, where $c \simeq 1.5\sigma^{-3}$ is the macroscopic bead number concentration and $c\Delta V$ is the average total number of beads in a region of volume ΔV. The quantity $\overline{\phi}_B(r)$ is an average of ϕ_B for a thin spherical annulus centered around the COM, averaged over time and over clusters with n in the chosen range.

Consider the increase of $\overline{\phi}_B(r = 0)$ at the cluster COM with increasing χN shown in Fig. 3(a). Note that the displayed values of χN are not evenly spaced. At $\chi N = 0$, the value of $\overline{\phi}_B(r = 0) \simeq 0.19$ is only slightly greater than spatial average value of $f = 0.125$, indicating the diffuse nature of these purely geometrical clusters. Upon increasing χN, $\overline{\phi}_B(r = 0)$ increases slowly for $\chi N < (\chi N)_{\mathrm{odt}}^{\mathrm{scf}}$, reaching approximately 0.4 at the next displayed value of $\chi N = 34.8$. The value
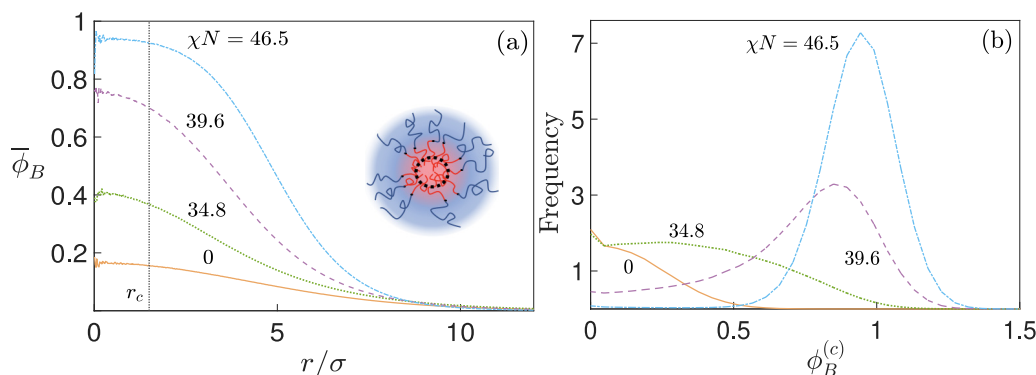

FIG. 3. (a) Local volume fraction $\overline{\phi}_B(r)$ of B (minority) block beads belonging to the cluster vs distance r from the center of mass of these beads, at $\chi N = 0$, 34.8, 39.6, and 46.5. (b) Probability distribution for the core volume fraction $\phi_B^{(c)}$ at the same χN values. The micelle schematic in (a) shows the inner core region of radius $r_c = 1.5\sigma$ used to define $\phi_B^{(c)}$.
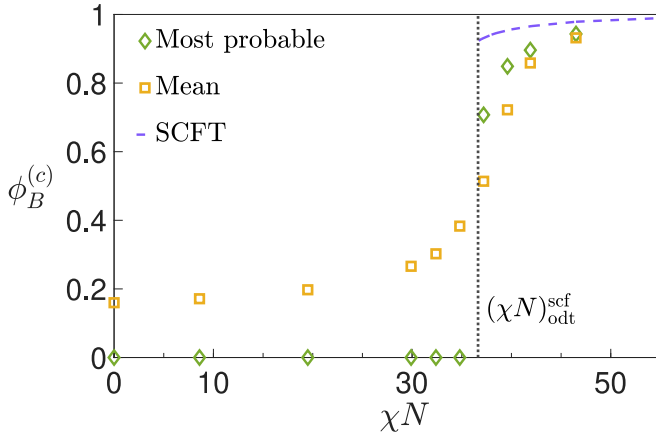
FIG. 4. Most probable (diamonds) and mean (square) values of the core volume fraction $\phi_B^{(c)}$ vs χN. The vertical dotted line indicates $\chi N = (\chi N)_{\text{odt}}^{\text{scf}} = 36.6$. The dashed blue line shows SCFT predictions for $\overline{\phi}_B(r = 0)$ for $\chi N > (\chi N)_{\text{odt}}^{\text{scf}}$.

$\overline{\phi}_B(r = 0)$ then increases much more rapidly from 0.4 to 0.8 over a much narrower range $\chi N = 34.8$-39.2 that includes $(\chi N)_{\text{odt}}^{\text{scf}} = 36.6$.

The average value $\overline{\phi}_B(r)$ shown in Fig. 3(a) presumably contain contributions both from diffuse geometrical clusters and from proper micelles with nearly pure B-rich cores. To distinguish these subpopulations, we have computed the probability distribution for the value of ϕ_B defined within a small spherical region of radius r_c around the COM. We refer to this quantity as the core volume fraction, denoted by $\phi_B^{(c)}$. We use a value $r_c = 1.5\sigma$, indicated by the vertical line in Fig. 3(a), giving $c\Delta V = 21.2$.

The probability distribution for $\phi_B^{(c)}$ is shown in Fig. 3(b) at several values of χN. At values of $\chi N = 0$ and 34.8 that are less than $(\chi N)_{\text{odt}}^{\text{scf}}$, we obtain a broad monotonically decreasing distribution that is very small at $\phi_B^{(c)} \simeq 1$, characteristic of diffuse geometrical clusters. At values of $\chi N > (\chi N)_{\text{odt}}^{\text{scf}}$, however, we observe a local maximum at a most probable value of $\phi_B^{(c)}$ that rapidly approaches 1 with increasing χN, indicating the appearance of proper micelles with a nearly pure core. Note that our definition of $\phi_B = m_B/c\Delta V$ leads to some instantaneous values $\phi_B^{(c)} > 1$, when the total number of beads in the sampled volume is less than the average $c\Delta V$.

Figure 4 shows the evolution of the mean and most probable values of the core volume fraction $\phi_B^{(c)}$ with χN. The discontinuous jump in the most probable value of $\phi_B^{(c)}$ from zero to a large nonzero value signals the appearance of a distinct population of proper micelles with a very B-rich core. Note that this jump in the most probable value with increasing χN occurs very near the value $\chi N = (\chi N)_{\text{odt}}^{\text{scf}}$, indicated by a vertical line.

We focus in this Letter primarily on the onset of micellization, rather than micelle crystallization. We have, however, attempted to place bounds on the ODT by running simulations of systems with $\chi N = 41.9$, 46.5, and 50.9 from disordered and artificially ordered initial states while monitoring for spontaneous crystallization and spontaneous melting,

respectively. These simulations were performed using periodic simulation unit cells designed accommodate $2 \times 2 \times 2$ or $3 \times 3 \times 3$ cubic unit cells of a bcc lattice (16 or 54 micelles), assuming a bcc unit cell length commensurate with the value of q^* measured in the disordered state at the same value of χN. In simulations designed for $3 \times 3 \times 3$ unit cells, we observed spontaneous melting for $\chi N = 41.9$ but never observed spontaneous crystallization. In simulations designed for $2 \times 2 \times 2$ unit cells, we observed spontaneous melting for $\chi N \leqslant 41.9$ and spontaneous crystallization for $\chi N = 46.5$ and 50.9. The evidence indicates an ODT value $(\chi N)_{\text{odt}} > 41.9$, though the exact value remains uncertain, and may be susceptible to finite-size effects. Further details of this study are given in the Supplemental Material [44].

The results presented here provide a clear picture of the appearance of disordered micelles within a model melt of asymmetric diblock copolymers. The most direct evidence for the appearance of micelles comes from a cluster analysis in which micelles are identified as geometrical clusters that contain a nearly pure core of minority block beads. The results indicate that such micelles appear over a rather narrow range of values of χN centered very near the SCFT ODT value. This conclusion is consistent both with the predictions of Wang and co-workers [10], who assumed the validity of SCFT predictions for the free energy of an isolated micelle, and with the results of previous simulation studies that have shown the somewhat surprising quantitative accuracy of SCFT predictions for properties of ordered phases and individual aggregates [16,17,43]. Our ability to make meaningful comparisons of simulations to SCFT predictions relied critically on the relatively recent development of improved methods for calibrating χ in simulation models [16,17]. To a very good approximation, it thus appears that the CMT in a melt of long, sphere-forming diblock copolymers corresponds to the SCFT ODT, and that the actual ODT occurs at a somewhat greater value of χN. We expect the onset of micellization at $\chi N \simeq (\chi N)_{\text{odt}}^{\text{scf}}$ to become more sudden with increasing $\overline{N}$, and for $(\chi N)_{\text{odt}}$ to decrease with increasing $\overline{N}$, but further study would be required to test these hypotheses.

Our computational results have several important implications for experiments. Our data for $S(q)$ provides useful insight into the interpretation of SAXS and SANS experiments [2,3,7], which indicates that identification of a CMT by scattering alone may be difficult in systems with experimentally relevant values of $\overline{N}$. In the systems studied here, for which the value of $\overline{N} = 3820$ is greater than in many experiments, the onset of micellization is signaled by the appearance of an initially small secondary shoulder in $S(q)$ and by an inflection in a plot $S^{-1}(q^*)$ vs χN, both of which arise from increased scattering associated with the appearance of micelles. Simulations of systems with lower $\overline{N}$, which we will report elsewhere, indicate that both features become less distinct with decreasing $\overline{N}$. Our comparison of results for $S(q)$ to the cluster analysis will aid the interpretation of future experiments. Our results are also consistent with experimental evidence for the existence of micelles over a significant range of temperatures, despite a remaining uncertainty regarding the location of the ODT for this simulation model. Our results establish that $(\chi N)_{\text{odt}}$ for this model

exceeds $(\chi N)_{\text{odt}}^{\text{scf}}$ by at least 14%, and possibly much more, since we were only able to establish a lower bound on $(\chi N)_{\text{odt}}$. Theory, experience with more symmetric diblock copolymers, and our own preliminary results for systems with lower $\overline{N}$ (to be presented elsewhere) all suggest that the difference $(\chi N)_{\text{odt}} - (\chi N)_{\text{odt}}^{\text{scf}}$ increases with decreasing $\overline{N}$. Further work is needed to determine the precise dependence of $(\chi N)_{\text{odt}}$ on $\overline{N}$, and to study dynamical processes in the disordered phase near the ODT, which are directly relevant to the remarkable history dependence seen in recent studies of phase transformations in sphere-forming diblock copoly-mers [31–33]. The present contribution provides a cornerstone for more detailed studies of the disordered micellar state by simulation.

[1] D. Kinning and E. Thomas, Macromolecules **17**, 1712 (1984).

[2] M. Schwab and B. Stühn, Phys. Rev. Lett. **76**, 924 (1996).

[3] M. Schwab and B. Stühn, Colloid Polym. Sci. **275**, 341 (1997).

[4] J. Adams, D. Quiram, W. Graessley, R. Register, and G. Marchand, Macromolecules **29**, 2929 (1996).

[5] J. K. Kim, H. H. Lee, S. Sakurai, S. Aid, J. Masomoto, S. Nomura, Y. Kitagawa, and Y. Suda, Macromolecules **32**, 6707 (1999).

[6] C. D. Han, N. Y. Vaidya, D. Kim, G. Shin, D. Yamaguchi, and T. Hashimoto, Macromolecules **33**, 3767 (2000).

[7] X. Wang, E. E. Dormidontova, and T. P. Lodge, Macromolecules **35**, 9687 (2002).

[8] J. N. Israelachvili, *Intermolecular and Surface Forces*, 3rd ed. (Academic, Amsterdam, 2011).

[9] E. E. Dormidontova and T. P. Lodge, Macromolecules **34**, 9143 (2001).

[10] J. Wang, Z.-G. Wang, and Y. Yang, Macromolecules **38**, 1979 (2005).

[11] G. H. Fredrickson and E. Helfand, J. Chem. Phys. **87**, 697 (1987).

[12] K. T. Delaney and G. H. Fredrickson, J. Phys. Chem. B **120**, 7615 (2016).

[13] M. W. Bates, J. Lequieu, S. M. Barbon, R. M. Lewis III, K. T. Delaney, A. Anastasaki, C. J. Hawker, G. H. Fredrickson, and C. M. Bates, Proc. Natl. Acad. Sci. U.S.A. **116**, 13194 (2019).

[14] T. M. Beardsley, R. K. W. Spencer, and M. W. Matsen, Macromolecules **52**, 8840 (2019).

[15] M. W. Matsen, J. Chem. Phys. **152**, 110901 (2020).

[16] J. Glaser, P. Medapuram, T. M. Beardsley, M. W. Matsen, and D. C. Morse, Phys. Rev. Lett. **113**, 068302 (2014).

[17] P. Medapuram, J. Glaser, and D. C. Morse, Macromolecules **48**, 819 (2015).

[18] M. Yadav, F. S. Bates, and D. C. Morse, Phys. Rev. Lett. **121**, 127802 (2018).

[19] T. Vidil, N. Hampu, and M. A. Hillmyer, ACS Central Sci. **3**, 1114 (2017).

[20] N. Hampu and M. A. Hillmyer, ACS Appl. Polym. Mater. **1**, 1148 (2019).

[21] N. Hampu, M. W. Bates, T. Vidil, and M. A. Hillmyer, ACS Appl. Nano Mater. **2**, 4567 (2019).

[22] N. Hampu and M. A. Hillmyer, ACS Macro Lett. **9**, 382 (2020).

[23] G. Ungar, Y. Liu, X. Zeng, V. Percec, and W.-D. Cho, Science **299**, 1208 (2003).

[24] X. Zeng, G. Ungar, Y. Liu, V. Percec, A. E. Dulcey, and J. K. Hobbs, Nature (London) **428**, 157 (2004).

[25] S. Lee, M. J. Bluemle, and F. S. Bates, Science **330**, 349 (2010).

[26] M. Huang, C.-H. Hsu, J. Wang, S. Mei, X. Dong, Y. Li, M. Li, H. Liu, W. Zhang, T. Aida, W.-B. Zhang, K. Yue, and S. Z. Cheng, Science **348**, 424 (2015).

[27] K. Yue, M. Huang, R. L. Marson, J. He, J. Huang, Z. Zhou, J. Wang, C. Liu, X. Yan, K. Wu, Z. Guo, H. Liu, W. B. Zhang, P. Ni, C. Wesdemiotis, W. B. Zhang, S. C. Glotzer, and S. Z. Cheng, Proc. Natl. Acad. Sci. U.S.A. **113**, 14195 (2016).

[28] S. A. Kim, K. J. Jeong, A. Yethiraj, M. K. Mahanthappa, J. Jeong, A. Yethiraj, and M. K. Mahanthappa, Proc. Natl. Acad. Sci. U.S.A. **114**, 4072 (2017).

[29] C. M. Baez-Cotto and M. K. Mahanthappa, ACS Nano **12**, 3226 (2018).

[30] Z. Su, C.-h. Hsu, Z. Gong, X. Feng, J. Huang, R. Zhang, Y. Wang, J. Mao, C. Wesdemiotis, T. Li, S. Seifert, W. Zhang, T. Aida, M. Huang, and S. Z. D. Cheng, Nat. Chem. **11**, 899 (2019).

[31] K. Kim, M. W. Schulze, A. Arora, R. M. Lewis III, A. Hillmyer, K. D. Dorfman, and F. S. Bates, Science **356**, 520 (2017).

[32] K. Kim, A. Arora, R. M. Lewis, M. Liu, W. Li, A.-C. Shi, K. D. Dorfman, and F. S. Bates, Proc. Natl. Acad. Sci. U.S.A. **115**, 847 (2018).

[33] S. Jeon, T. Jun, S. Jo, H. Ahn, S. Lee, B. Lee, and D. Y. Ryu, Macromol. Rapid Commun. **40**, 1900259 (2019).

[34] L. Leibler, Macromolecules **13**, 1602 (1980).

[35] M. W. Matsen and M. Schick, Phys. Rev. Lett. **72**, 2660 (1994).

[36] G. H. Fredrickson, *The Equilibrium Theory of Inhomogeneous Polymers* (Clarendon, Oxford, UK, 2006).

[37] G. M. Grason, B. A. DiDonna, and R. D. Kamien, Phys. Rev. Lett. **91**, 058304 (2003).

[38] N. Xie, W. Li, F. Qiu, and A. C. Shi, ACS Macro Lett. **3**, 906 (2014).

[39] P. Grzywacz, J. Qin, and D. C. Morse, Phys. Rev. E **76**, 061802 (2007).

[40] D. C. Morse and J. K. Chung, J. Chem. Phys. **130**, 224901 (2009).

[41] J. Glaser, J. Qin, P. Medapuram, and D. C. Morse, Macromolecules **47**, 851 (2014).

[42] T. Ghasimakbari and D. C. Morse, Macromolecules **51**, 2335 (2018).

[43] T. Ghasimakbari and D. C. Morse, Macromolecules **53**, 7399 (2020).

[44] See Supplemental Material at http://link.aps.org/supplemental/10.1103/PhysRevMaterials.5.L092601 for further details of MD simulations and analysis.